EUROPEAN ORGANIZATION FOR NUCLEAR RESEARCH

CERN-EP/87-132
27.7.1987

Isotope Shift and Hyperfine Structure of Stable Platinum Isotopes*

W. Neu+ and G. Passler
Institut für Physik, Universität Mainz, Federal Republic of Germany

G. Sawatzky and R. Winkler
Optisches Institut, Technische Universität Berlin, Federal Republic of Germany

H.-J. Kluge
Institut für Physik, Universität Mainz and CERN, ISOLDE Collaboration, Geneva, Switzerland

submitted to Z. Phys. D.

July 1987

---

* Dedicated to Professor Siegfried Penselin on the occasion of his 60th birthday.

+ Present address: CERN, CH-1211 Geneva 23, Switzerland

Abstract: Isotope shift (IS) and hyperfine structure (hfs) measurements have been performed on seven lines of the platinum I spectrum with interference as well as laser fluorescence spectroscopy. In the latter case a frequency-doubled single-mode cw dye laser was applied. The IS of ^{190}Pt with a natural abundance of only 0.01% was determined to be $\delta\nu^{190/192}$ = -38.65(8) mK in the λ306.47 nm transition. The IS parameters and the effective hfs integrals in the configuration $(5d + 6s)^{10}$ were determined in intermediate coupling by a least squares fit of the IS and hfs data with eigenvectors obtained from the platinum fine structure (fs). The results are compared with theoretical values and yield improved $\delta\langle r^2\rangle$ data.

1. Introduction

Optical isotope shift (IS) and hyperfine structure (hfs) measurements on platinum (Z = 78) have been performed by several groups for more than 50 years. The optical data are used to test atomic theory and to deduce nuclear moments and changes in the nuclear mean square charge radius $\delta\langle r^2\rangle$. The method of hollow-cathode spectroscopy provided a large number of IS and hfs data of the six stable isotopes of platinum in several optical transitions [1 - 5]. Recent atomic-beam magnetic-resonance (ABMR) measurements of Büttgenbach et al. [6] and Greenebaum et al. [7] yielded very precise data on the magnetic hfs constant A for the ground state $5d^96s\ ^3D_3$ and the first metastable states $5d^96s\ ^3D_2$ and $5d^86s^2\ ^3F_4$.

The present measurements on platinum were performed in order to improve the accuracy and to provide some new IS and hfs data. Until now, little information has been available on the IS of ^{190}Pt due to its very low abundance (0.01 %) in the natural isotopic mixture. The only IS measurement on this isotope has been done in the transition $5d^96p\ ^3P_2 \rightarrow 5d^86s^2\ ^3F_3$ (λ444.25 nm) with a rather high uncertainty [3]. Furthermore, the IS in this line is difficult to interpret because of the simultaneous transition of two electrons.

Figure 1 shows part of the level scheme of Pt I. The numbers given in parentheses are the branching ratios of the fluorescence decay [8]. The lifetimes of the excited levels are also included as far as they are known [9]. This shows clearly that the strongest transition with λ306.47 nm is the most suitable line for a determination of the IS of ^{190,192}Pt. Furthermore, it represents an s → p transition which is rather easy to interpret.

2. The experimental technique

This work represents an application of the technique of resonance-fluorescence spectroscopy on a thermal, collimated atomic beam and of interference spectroscopy on a hollow-cathode discharge. In order to perform high-resolution spectroscopy in the ultraviolet (UV) optical lines at $\lambda \approx 300$ nm, a frequency-doubled continuous wave (cw) dye laser was used. The experimental setup is shown in Fig. 2. The optical transitions outside the $\lambda \approx 300$ nm region were studied by interference spectroscopy. The basic apparatus consists of a hollow cathode as light source, a Fabry-Pérot interferometer as spectrometer, and a photomultiplier with single-photon counting. Since it has already been described in detail in [4, 10], only the laser setup is reported in the following.

2.1 The setup for laser spectroscopy

The atomic-beam apparatus: The crucial part of the atomic-beam apparatus is the platinum oven. Among the possible oven materials which stand the required high evaporation temperatures, carbon is the only one which does not alloy with Pt. The carbon crucible, cylindrically shaped with a length of $l = 18$ mm and a diameter of $d = 6$ mm, is heated by electron bombardment. This allows high oven temperatures, up to 3300 °C. The collimation of the atomic beam is performed by a long, cylindrical channel ($l = 8$ mm, $d = 1$ mm) through which the platinum atoms are evaporated within a cone of about 14° full angle. This method of collimation has the advantage of a low consumption of Pt, while the number of atoms emerging in the direction

of the tube remains undiminished [11]. The reservoir of the oven is filled with about 10 mg of platinum, which is sufficient to perform all the measurements described.

The platinum oven, surrounded by heat shields to reduce the energy dissipation by radiation, is mounted in a water-cooled vacuum chamber. The atomic beam enters the chamber, where it interacts with the laser beam, through a hole with a diameter of 3 mm. Both chambers are pumped separately. The interaction region of the atomic and the laser beam is imaged by a lens system, with a magnification factor of 3, onto the photocathode of the photomultiplier. The black-body radiation of the oven is blocked by a coloured-glass filter. The effective solid angle of observation, including all reflection and absorption losses, is about 7% of 4π. To reduce the background signal produced both by stray light from the laser beam and black-body radiation of the hot oven, the entire interaction chamber is blackened, several light traps are installed to avoid reflections, and the laser beam enters and exits the interaction chamber through two long tubes in which diaphragms are placed. The laser entrance and exit windows are set to the Brewster angle to minimize reflection losses.

These efforts result in the following typical count rates: the dark rate of the photomultiplier itself is 24 Hz; the hot oven produces a rate of about 30 Hz (T = 3000 °C) and the laser (P_{UV} = 0.4 mW) about 30 Hz. Altogether the background rate sums up to ≈ 90 Hz.

The laser and frequency doubling system: The laser system used is a commercial linear single-mode cw dye laser (Coherent CR599/21) pumped by an argon-ion laser. Within the tuning range of Rhodamin 6G almost all transitions of Pt I in the $\lambda \approx 300$ nm region can be studied. Although powerful

lasers have been developed during recent years, frequency doubling suffers from the available output power of cw systems. Therefore the output of the actively stabilized dye laser is coupled into an external optical resonator containing the frequency-doubling crystal. Hence the available UV power is increased by the square of the quality of the optical resonator. The resonator is built up as a ring cavity with four dielectric mirrors, one mounted on a piezo crystal (PZT). By applying a voltage up to 1000 V one can use this PZT to tune the length of the resonator. The resonator length is stabilized to an integer number of the laser wavelength by a method developed by Hänsch and Couillaud, who give a detailed description of the stabilization scheme [12]. In order to make use of the enhanced power inside the external resonator and to reach the highest possible power density, the frequency-doubling crystal is placed at a focus of the cavity. The produced UV beam is coupled out by a dichroic beam splitter. The resonance enhancement inside the cavity with the crystal and the dichroic beam splitter in place is typically of the order of 10-12, which results in an enhancement of the UV intensity by a factor of about 100-150.

Except for the use of $LiIO_3$ as a frequency-doubling crystal, the method of frequency-doubling of a cw dye laser as described above, has been applied by several groups [13 - 16]. Two recent publications reported the use of a $LiIO_3$ crystal placed inside the laser resonator of a ring dye laser [17, 18]. A $LiIO_3$ crystal has been chosen as frequency doubler in this work because it is the most efficient crystal in the tuning range of Rhodamin 6G [16, 19] Experiments with the $LiIO_3$ and the usually used temperature-tuned ammonium dihydrogen arsenate (ADA) crystal showed the superiority of the $LiIO_3$. For $LiIO_3$ the phase matching between the ground wave and the second harmonic is achieved by tuning the angle of beam propagation to

the optical axis of the crystal. This led to a very stable output power but also to a non-Gaussian beam profile of the UV beam. This problem was solved by appropriate beam optics. Tests with an ADA crystal showed a good UV beam profile. However, the temperature has to be stabilized to better than 0.01 °C in order to obtain a constant frequency-doubling efficiency. This was difficult to achieve with the crystal placed in the focus of the ring resonator. The absorption of the ADA crystal in the UV and visible caused a temperature gradient which was hard to compensate.

The $LiIO_3$ crystal is cut at the Brewster angle to minimize the reflection losses inside the cavity. The dichroic beam splitter is also mounted at the Brewster angle. Its transmission for the ground wave is $\geq$ 98% while, at the same time, a high reflectivity of about 95% is achieved for the UV laser beam.

The tuning range of the $LiIO_3$ is about 13 nm in the UV, limited by the growing losses due to the tilting of the crystal to fulfil the phase-matching condition. A larger tuning range can be achieved by using several crystals, each cut at a different angle with respect to the optical axis. The maximum UV power obtained in this experiment was about 1.5 mW at $\lambda \approx 300$ nm at 300 mW dye-laser output.

The wavelength of the dye laser is set at $2\lambda_{res}$ with the help of a Burleigh wavemeter. The molecular absorption spectrum of iodine, tabulated in Ref. [20], is recorded simultaneously to give an absolute frequency scale. A Fabry-Pérot etalon with a free spectral range (FSR) of 300 MHz provides relative frequency marks.

3. Measurements and results

As indicated in Fig. 1, measurements were performed in six lines linking the ground configurations $5d^96s^2$ and $5d^96s$ to the excited $5d^96p$ levels and in the λ304.26 nm transition which leads to the $5d^86s6p\ ^5G_5$ fine structure (fs) level. In order to obtain high-quality data for a determination of the changes of the nuclear mean square charge radii $\delta\langle r^2\rangle$ of the Pt isotopes, as many isotopes as possible were investigated by high-resolution laser fluorescence spectroscopy. To improve the parametric description of the IS in platinum, interference spectroscopy was applied to as many transitions as possible originating from the $(5d + 6s)^{10}$ ground configurations. Because of the limited resolution of this technique, the investigations of the IS were restricted to the most abundant even-even isotopes ^{194}Pt and ^{196}Pt.

Figure 3 shows a spectrum of Pt I obtained by laser spectroscopy in the transition $5d^96s\ ^3D_3 \rightarrow 5d^96p\ ^3P_2$ (λ306.47 nm). The full width at half maximum is about 70 MHz, mainly due to the residual Doppler broadening (≈ 60 MHz) of the atomic beam. The isotope of lowest abundance, ^{190}Pt, is only visible after a magnification of the intensity scale by a factor of 500 (inset of Fig. 3).

A calibration of the laser frequency via the absorption spectrum of molecular iodine produces rather large uncertainties. Therefore the frequency scale was obtained with the help of the very precisely measured hyperfine splitting of ^{195}Pt in the $5d^96s\ ^3D_{3,2}$ [6] and the $5d^86s^2\ ^3F_4$ [7] levels. The frequency marks of the Fabry-Pérot etalon provide the frequency scale between the hfs resonances.

Table 1 compiles the IS data of the transitions involving the $(5d + 6s)^{10}$ ground-state configurations and compares the present data with those given in the literature. Generally the more precise values of this work agree with the former ones. The IS of ^{190,192}Pt is determined in the strong optical transition $5d^9 6s\ ^3D_3 \rightarrow 5d^9 6p\ ^3P_2$ (λ306.47 nm). For the λ300.22 nm line, the very first IS data are obtained by the present work.
The only stable isotope showing a hyperfine splitting is ^{195}Pt ($I = 1/2$). The A factors for all transitions studied are summarized in Table 2 together with the values given in the literature [3, 4, 6, 7]. With the exception of $A(5d^9 6p\ ^3F_3)$ the agreement of the values obtained in this work with earlier measurements is good.

4. Discussion

The large number of hfs and IS data available for Pt allows a study of the $(5d + 6s)^{10}$ ground configurations in terms of effective hyperfine radial integrals and a parametric descriptions of the IS. For this, the eigenvector components have to be determined from an investigation of the fs.

4.1 Fine structure parameters and g_J values

The $(5d + 6s)^{10}$ electrons of Pt have the three configurations $5d^8 6s^2$, $5d^9 6s$, and $5d^{10}$, which give rise to 14 closely lying fs levels. Twelve of these are experimentally known. The two missing levels have $J = 0$. Hence

the eigenvector components of $5d^{10}\ ^1S_0$, the only observed fs level with $J = 0$, cannot be determined in a unique way. Therefore only 11 levels actually remain for a fs fit. Similar to the calculation of Büttgenbach [6], the effective electrostatic spin-orbit (EL-SO) interaction [21] is taken into consideration as well as the usually included electrostatic and magnetic interactions. However, the small contribution of the Q^4 integral of the effective EL-SO interaction is neglected in order to reduce the number of free parameters. The resulting fs parameters are compiled in Table 3. Using these parameters the fs energies can be recalculated with a mean square deviation of $\sigma = 20\ cm^{-1}$, which is only 0.08% of the energy range considered. The calculation of the g_J factors provides a further sensitive test of the intermediate coupling eigenfunctions. It can be seen from Table 4 that the agreement is good. In comparison with the results of Ref. [6], our results for the fs energies are slightly worse whereas our g_J values are slightly better. The remaining ambiguity of the eigenvector components is due to the limited number of available level energies which makes it difficult to fix completely the interaction parameters. In any case, the accuracy of the eigenvector components calculated should be sufficient for the following hfs and IS analysis.

4.2 Hyperfine structure

The improved accuracy of the A factors within the $(5d + 6s)^{10}$ configurations of Pt calls for a recalculation of the magnetic hfs by the effective operator technique developed by Sandars and Beck [22]. The eleven measured A factors of the $5d^96s^2$ and $5d^96s$ configurations can be expressed as

a linear combination of seven a^{kskl} factors. Using our eigenvector components (see Section 4.1) and following a procedure similar to the one of Büttgenbach et al. [6], the number of effective radial integrals, or a^{kskl} factors, is reduced to only four. When linear combinations of these effective hfs constants are adjusted to all eleven experimental A factors, rather large discrepancies ($\chi = \Sigma\ |A_{exp} - A_{calc}| = 86$ mK) are obtained, especially for the strongly mixed fs levels with J = 2. Omitting these J = 2 levels in the adjustment one obtains much better results ($\chi = 46$ mK for all eleven A factors). Obviously the levels with J = 2, especially $5d^96s\ ^3D_2$, are disturbed. The resulting effective 'a' factors, which comprise relativistic as well as configuration mixing effects, are compiled in Table 5. They are compared with the evaluation of Büttgenbach et al. [6], a multi-configuration Dirac-Fock (MCDF) [23] and an optimized Hartree-Fock-Slater (OHFS) calculation [24]. As can be seen from Table 5, a substantial improvement in consistency is obtained for $a^{12}(d)$. With the exception of $a^{10}(d)$ the magnetic hfs factors are so well fixed that the remaining small discrepancies must be attributed to deficiencies of the self-consistent calculations and/or the truncation of the effective operator description to four parameters.

Using the parameters of Table 5 for a recalculation of the A factors within the $(5d + 6s)^{10}$ configurations, one obtains the values given in Table 6. They are compared with the experimental values. As expected, good agreement is obtained, except for some J = 2 levels where strong configuration interaction takes place and the magnetic hfs is very sensitive to the eigenvector components and to neglecting the direct hfs interaction between the $5d^86s^2$ and the $5d^96s$ configuration.

4.3 Isotope shift

The IS can be described as the sum of the field shift (FS) and the mass shift (MS) (see, for example works by King [25, 26]). The FS arises from the electrostatic interaction between the finite nuclear charge distribution and the electrons near the nucleus. Therefore the FS can be used to determine the change of the nuclear charge distribution between two isotopes. The MS is the sum of the normal mass shift (NMS) and the specific mass shift (SMS). While the NMS can be calculated easily by introducing the reduced mass, the SMS depends on the correlation of the electron momenta and is difficult to calculate.

Non-relativistic first-order perturbation theory yields one IS value for all pure levels of a configuration. Configuration interaction is taken care of by the sharing rule. Ab-initio calculations of the FS only give reliable results for simple level schemes such as those of the alkalies and of the alkaline-earths [27]. In cases where complex configurations lie close together and are well separated from other disturbing configurations, the parametric description of the IS is appropriate [28, 29]. This applies to the case of the $(5d + 6s)^n$ low-lying configurations of W through Pt [30 - 32]. With the more accurate data of the present work, a re-examination of the parametric description of the IS of Pt [5] follows. According to Bauche [28], the IS (corrected for the NMS) of an atomic level relative to any reference level can be expressed as a linear combination of first- and second-order parameters. The first-order parameter 'a' describes the FS and the SMS of the reference level; the parameter 's' those between the $5d^96s$ and $5d^86s^2$ levels. The coefficient of 'a' is unity in all cases and that of 's' can be calculated from the eigenvector components determined in Section 4.1.

Entering into the next order are the crossed-second-order (CSO) parameters which are derived from effective-operator products between IS and electrostatic and magnetic fs operators. The SMS for heavy elements such as Pt is small in respect to the field shift. Hence it is neglected in second order leading to the CSO effects being described by four additional parameters g_2, h, $z(5d^86s^2)$, and $z(5d^96s)$, which have the same angular coefficient as the fs radial integral G_2, the configuration interaction parameter $H = (1/35)R^2(dd,ds)$ [33], and the spin-orbit radial integrals ζ for the corresponding configurations.

In order to reduce the number of free parameters, only the ISs within the $(5d + 6s)^{10}$ configurations are considered. Hence the 'a' parameter is eliminated. A further reduction is obtained by using $z(5d^86s^2)/z(5d^96s) = \zeta(5d^86s^2)/\zeta(5d^96s)$, which is justified because of the small contributions of the 'z' parameters. Hence the linear combinations of four parameters can be adjusted to the five ISs within the $(5d + 6s)^{10}$ configurations which are calculated from the measured IS values given in Table 1. The resulting parameters are compiled in Table 7 and compared with the earlier result [5]. The present values are about four times as accurate and describe very well the observed IS, as can be seen from Table 8. The only strong deviation from the results of Ref. [5] is observed for the parameter g_2. This is also the only one which can be compared with a theoretical value. Since g_2 describes the FS between pure terms, the FS between $5d^96s\ ^1D$ and ^3D can be written according to the theorem of van Vleck [33] as $\Delta FS(^3D - ^1D) = -2g_2$. Aufmuth performed a Hartree-Fock (HF) calculation of the FS and obtained $\Delta FS(^3D - ^1D) = 11.2\ 10^{-3}\ cm^{-1}$ which yields $g_2^{HF} = -5.6\ 10^{-3}\ cm^{-1}$ [34], in excellent agreement with our experimental value given in Table 7. The perfect coincidence of experi-

mental and recalculated IS values within the experimental errors (Table 8) demonstrates the ability of the parametric method to describe the IS in complex configurations. The information available in the W-Pt region enables a study of possible systematics of the IS parameters and may stimulate further theoretical work.

5. Changes in nuclear charge radii

The consistent description of the IS in the $5d^86s^2$ and $5d^96s$ configurations by the parametric method allows a calculation of differences in nuclear charge radii. Since the parameter 's' describes the FS and SMS of these pure configurations, it can be expressed as

$$s^{194,196} = SMS^{194,196}(5d^86s^2 \rightarrow 5d^96s) + (a_0^3/Z)\Delta|\psi(0)|^2 f(z) \delta \lambda^{194,196}.$$

The second term in the sum is the well-known formula of the FS [35] including the screening ratio δ. Wilson [36] carried out the calculation of the SMS using pseudo-relativistic wave functions. He obtained $SMS(5d^96s \rightarrow 5d^86s^2)^{194,196} = 3.8\ 10^{-3}cm^{-1}$, in agreement with the value $3(2)\ 10^{-3}cm^{-1}$ given in Ref. [29]. The electron charge density at the nucleus $|\psi(0)|^2_{5d^96s}$ can be obtained from $a^{10}(s)$ (Table 5) with the help of the Goudsmit-Fermi-Segrè formula [37]. With $|\psi(0)|^2 = 17.05\ a_0^{-3}$ one obtains $\lambda^{194,196} = 0.044(1)\ fm^2$, where $f(Z) = 2.0091\ cm^{-1}/fm^2$ and $\delta = 2.08$ [35] are used. This result, using IS data corrected for CSO effects, is in fair agreement with $\lambda^{194,196} = 0.053(6)\ fm^2$ [35], where the weighted mean value of corrected and uncorrected IS values was used. It is difficult to decide which value should be favoured. The situation should clarify when

IS data become available for a longer series of Pt isotopes. Since the nuclear deformation of the Pt, Au, and Hg isotopes are rather well known, the charge radii can be corrected for changes in deformation. Then the slopes of the λ values of Pt, Au, and Hg isotopes should be almost identical, i.e. described by the droplet model which is a modification of the liquid drop model [38].

The laser measurements yielded quite accurate IS data, especially for the lightest stable isotope ^{190}Pt. Hence, an improved set of λ values can be given. In order to avoid the uncertainties in absolute values, we give the data relative to the isotope pair $^{196/198}$Pt, where the IS has been determined in this work with the highest accuracy. A King plot [25] allows a combination of the measurements performed in different optical lines so as to check their consistency. Figure 4 shows an example. The measured IS minus the NMS of two optical transitions i,j related to the isotope pair $^{194/196}$Pt are plotted against each other and fitted by a straight line. For the straight-line fit only the even isotopes have been taken into account. The data points including ^{195}Pt show the consistency of all data. This kind of King plot [26] has the advantage that all values are of the same order of magnitude as the measured IS values. The slope of the resulting straight line gives the ratio of the electronic factors in both lines F_i/F_j. The intersection with the ordinate gives the quantity $\Delta SMS = SMS_i^{194/196} F_i/F_j - SMS_j^{194/196}$. All values obtained by combining two lines at a time are given in Table 9. The SMSs in all $s \rightarrow p$ and $ns^2 \rightarrow nsnp$ transitions investigated are in good agreement, within the estimated error, with the values of Heilig and Steudel [39], which are (0.3 ± 0.9)NMS and (0 ± 0.5)NMS respectively. The correlations of data in different lines from the various King plots and the estimates of Heilig and

Steudel can be used to determine the SMS of the λ300.22 nm line for the isotope pair $^{194/196}$Pt. This yields the value $\Delta\nu^{SMS} = 9.4(1.5)\ 10^{-3}\ cm^{-1}$, which is about ten times that of the NMS.

Owing to the fact that no absolute value of at least one of the electronic factors F_i is known, no absolute values of the nuclear parameter $\lambda^{A,A'} \approx \delta\langle r^2\rangle^{A,A'}$ are given in the following. By defining $\lambda^{196/198}{}_{rel} = 1$ for the most precisely measured ISs of $^{196/198}$Pt one obtains the values of the relative nuclear parameter $\lambda^{A,A'}{}_{rel}$ as given in Table 10. For comparison, those given by [35] are also included. A significant improvement of accuracy is obtained, especially for ^{190}Pt.

Acknowledgement

We thank M. Wilson for his calculation and S. Buettgenbach, B. Fricke, and K. Heilig for stimulating discussions. The laser experiments were supported by the Deutsche Forschungsgemeinschaft.

References

[1] B. Jaeckel: Z. Phys. 100, 513 (1936)

[2] V. Stacey, H.G. Kuhn: Proc. R. Soc. A322, 301 (1971)

[3] P.E.G. Baird, D.N. Stacey: Proc. R. Soc. A341, 399 (1974)

[4] G. Müller, R. Winkler: Z. Phys. A273, 313 (1975)

[5] H. Grethen, R. Winkler, J. Bauche: Physica 98C, 222 (1980)

[6] S. Büttgenbach, N. Gläser, B. Roski, F. Traber: Z. Phys. A317, 237 (1984)

[7] G. Greenebaum, W.J. Childs, L.S. Goodman: Bull. Am. Phys. Soc. 16, 532 (1971)

[8] J. Lotrian, Y. Guern: J. Phys. B15, 69 (1982)

[9] D.S. Gough, P. Hannaford, R.M. Lowe: J. Phys. B15, L431 (1982)

[10] B. Buchholz, K, Dörschel, R. Winkler: J. Phys. E14, 828 (1981)

[11] P. Clausing: Z. Phys. 66, 471 (1930)

[12] T.W. Hänsch, B. Couillaud: Opt. Commun. 35, 444 (1980)

[13] M. Brieger, H. Büsener, A. Hese, F.v. Moers, A. Renn: Opt. Commun. 38, 423 (1981)

[14] L.A. Bloomfield, H. Gerhardt, T.W. Hänsch, S.C. Rand: Opt. Commun. 42, 247 (1982)

[15] J.C. Bergquist, H. Hemmati, W.M. Itano: Opt. Commun. 43, 437 (1982)

[16] A. Renn, A. Hese, H. Büsener: Laser and Optoelektronik 3, 11 (1982)

[17] W.A. Majewski: Opt. Commun. 35, 201 (1985)

[18] T.F. Johnston, T.J. Johnston: Laser spectroscopy VI. In: Springer Ser. Opt. Sci. Vol. 40, p. 417. Eds. H.P. Weber and W. Luety

(Springer, Berlin-Heidelberg 1983); Coherent, Inc. Information sheet

[19] H. Büsener, A. Renn, M. Brieger, F.v. Moers, A. Hese: Appl. Phys B39, 77 (1986)

[20] S. Gerstenkorn, P. Luc: Atlas du spectre d'absorption de la molecule d'iode. Lab. Aime-Cotton, 1980

[21] Z.B. Goldschmidt: Handbook on the physics and chemistry of rare earth. Eds. K.A. Gschneider Jr. and L. Eyring (North-Holland, Amsterdam 1978)

[22] P.G.H. Sandars, J. Beck: Proc. Roy. Soc. A289, 97 (1965)

[23] S. Büttgenbach (ed.): Hyperfine structure in 4d and 5d shell atoms. In: Springer Tracts in Modern Physics. Vol. 96. (Springer, Berlin-Heidelberg-New York 1982)

[24] G. Olsson, A. Rosen: Phys. Scr. 26, 168 (1982)

[25] W.H. King: J. Opt. Soc. Am. 53, 822 (1963)

[26] W.H. King: Isotope shifts in atomic spectra. Physics of atoms and molecules. (Plenum Press, New York-London 1984)

[27] G. Torbohm, B. Fricke, A. Rosen: Phys. Rev. A31, 2038 (1985)

[28] J. Bauche, Thesis, C.N.R.S., Orsay 1969

[29] J. Bauche, R.-J. Champeau: Adv. Atom. Mol. Phys. 12, 39 (1976)

[30] E. Wöbker, Thesis, Hanover 1985

[31] J.R. Kropp, H.D. Kronfeldt, A. Lucas, R. Winkler: Physica 138, 335 (1986)

[32] G. Sawatzky, R. Winkler: to be published

[33] E.K. Condon, H. Odabasi: Atomic structure. (Cambridge University Press. 1980)

[34] P. Aufmuth: J. Phy. B15, 3127 (1982)

[35] P. Aufmuth, K. Heilig, A. Steudel: to be published in At. Data Nucl. Data Tables

[36] M. Wilson, private communication

[37] H. Kopfermann: Nuclear moments. (Academic Press, New York 1958)

[38] W.D. Myers, K.-H. Schmidt: Nucl. Phys. A410, 61 (1983)

[39] K. Heilig, A. Steudel: At. Data Nucl. Data Tables 14, 613 (1974)

[40] H. Grethen: Diploma work, Berlin 1976 (unpublished)

Table 1:

Isotope shifts $\delta\nu^{A,A'}$ of stable Pt isotopes in transitions originating from the $(5d + 6s)^{10}$ ground configurations. The upper part gives the data of the transitions studied by laser spectroscopy, whereas the other lines (lower part) were investigated by interference spectroscopy. The λ444.25 nm and λ522.76 nm transitions were investigated earlier and their data are included for completeness.

$\delta\nu^{A,A'}$ [10^{-3} cm^{-1}]						
Optical transition [nm]	A,A' 190,192	192,194	194,195	194,196	196,198	Ref.
299.79	-	-54.4(1.2)	-26.09(9)	-56.43(44)	-60.81(44)	This work
	-	-	-	-60(5)	-	[1]
300.22	-	-138.57(36)	-65.25(7)	-142.44(38)	-154.58(40)	This work
304.26	-	-84.22(29)	-39.79(17)	-86.62(18)	-93.28(19)	This work
	-	-84.7(1.5)	-39.5(9)	-86.4(5)	-94.3(9)	[2]
	-	-87.6(7.0)	-40.3(1.4)	-87.33(40)	-94.67(48)	[3]
306.47	-38.65(8)	-43.19(56)	-20.24(60)	-43.62(56)	-47.73(12)	This work
	-	-	-	-45	-	[1]
270.24	-	-	-	-72.5(1.5)	-	This work
	-	-	-	-76	-	[1]
411.86	-	-	-	-79.06(84)	-	This work
	-	-	-	-79(2)	-	[4]
416.45	-	-	-	-147.6(9)	-	This work
	-	-	-	-145(3)	-	[4]
444.25	-	-	-	-165.1(4)	-	[2]
522.76	-	-	-	-83(1)	-	[4]

Table 2:

Compilation of A factors of ^{195}Pt in transitions studied in this work. $A(^3D_3)$, $A(^3D_2)$, and $A(^3F_4)$ given by Refs. [6, 7] were used for the frequency calibration of the spectra obtained by laser spectroscopy.

A-factors [10^{-3} cm^{-1}]					
Level		This work	Refs. [6, 7]	Ref. [3]	Ref. [4]
$5d^96s$	$^3D_3$	-	190.2198(8)	-	-
	$^3D_2$	-	-87.0485(1)	-	-
	$^3D_1$	-168(2)	-	-	-176(5)
	$^1D_2$	185.0(5)	-	-	-182(3)
$5d^86s^2$	$^3F_4$	-	28.3201(1)	-	-
	$^3P_2$	69.6(5)[a]	-	-	66(2)
	$^3F_3$	40.8(6)	-	41.3(1.2)	36(3)
	$^3F_2$	55(8)[b]	-	-	45(8)
	$^1G_4$	43(2)[b]	-	-	37(3)
$5d^96p$	$^3P_2$	61.72(16)	-	61.8(1.2)	60(1)
	$^3F_3$	102.53(15)	-	-	95(3)
	8_3	64.9(5)	-	-	63(1)
$5d^86s6p$	$^5G_5$	126.53(13)	-	127.3(4)	-
	22_3	60.9(1.5)[b]	-	-	57(3)

[a] Ref. [40]

[b] Reevaluated from Ref. [4] with the new results of this work.

Table 3:

Fine structure parameters of the $5d^86s^2$ and $5d^96s$ configurations of Pt in units of cm^{-1}. A is an additive constant to all levels of a configuration.

Parameter	$5d^86s^2$	$5d^96s$
A	16483	6762
$F^2(d,d)$	49007	
$F^4(d,d)$	37264	
$G^2(d,s)$		13547
$H = (1/35)R^2(dd,ds)$	547	
ζ	4254	4041
α	25	
Q^2	-620	

Table 4:

Experimental and calculated g_J values of the $(5d + 6s)^{10}$ ground configurations. The eigenvector components of Table 3 are used.

g_J values			
Level		Exp.	Calc.	Exp. - Calc.
$5d^8 6s^2$	$^3P_1$	-	1.50116	-
$5d^9 6s$	$^3D_1$	-	0.49884	-
$5d^9 6s$	$^3D_2$	1.06657	1.06773	-0.00116
$5d^8 6s^2$	$^3P_2$	1.11691	1.11712	-0.00021
$5d^9 6s$	$^1D_2$	1.17	1.18416	-0.014
$5d^8 6s^2$	$^3F_2$	0.92	0.97208	-0.05
$5d^8 6s^2$	$^1D_2$	0.97	0.99303	-0.02
$5d^9 6s$	$^3D_3$	1.33392	1.33411	-0.00019
$5d^8 6s^2$	$^3F_3$	-	1.08353	-
$5d^8 6s^2$	$^3F_4$	1.23948	1.24000	-0.00052
$5d^8 6s^2$	$^1G_4$	-	1.01058	-

Table 5:

Effective $a^{kskl}(l)$ factors given in 10^{-3} cm^{-1} in the $(5d + 6s)^{10}$ configurations of Pt.

Conf.		Experimental		Theoretical	
		This work	Ref. [6]	MCDF [6]	OHFS [24]
$5d^8 6s^2$	$a^{10}(d)$	1(6)	-9	-5	-5
	$a^{01}(d)$	42(1)	44	46	47
	$a^{12}(d)$	51(8)	17	58	60
$5d^9 6s$	$a^{10}(s)$	1008(3)	981	878	1044

Table 6:

A factors of the $(5d + 6s)^{10}$ configuration of Pt. The experimental values (taken from Table 2 and Ref. [4]) are compared with those calculated by the help of the effective a^{kskl} factors of Table 5.

A-factors [10^{-3} cm^{-1}]				
Level		Exp.	Calc.	Exp. - Calc.
$5d^9 6s$	$^3D_1$	-168(2)	-167.6(4.5)	-0.5
	$^3D_3$	190.2198(8)	190.2(1.4)	0.02
$5d^8 6s^2$	$^3P_1$	-5(10)	-4(5)	-1
	$^3F_3$	40.8(6)	40.1(1.1)	0.7
	$^3F_4$	28.3201(1)	28.3(1.7)	0.02
	$^1G_4$	43(2)	43.9(1.1)	-0.9
$5d^9 6s$	$^3D_2$	-87.0485(1)	-97.6(3.5)	10.6
	$^1D_2$	185.0(5)	182.9(3.0)	2.1
$5d^8 6s^2$	$^3P_2$	69.6(5)	88.6(1.5)	-19.0
	$^3F_2$	55(8)	53(2)	2
	$^1D_2$	65(10)	69(4)	-4

Table 7:

Isotope shift parameters of Pt in the $5d^9 6s$ and $5d^8 6s^2$ configurations in units of 10^{-3} cm^{-1}. The errors given are the standard deviations resulting from the least squares fit.

Parameter	This work	Ref. [5]
s	-122.7(2)	-117(4)
g_2	-4.7(2)	-15(6)
h	-1.46(3)	-1.4(7)
$z(5d^9 6s)$	2.12(8)	2.0(2.1)

Table 8:

Experimental and recalculated isotope shifts between ^{194}Pt and ^{196}Pt in the $5d^9 6s$ and $5d^8 6s^2$ configurations in units of 10^{-3} cm^{-1}. The IS values are corrected for the contribution of the normal mass shift.

Levels				$(IS-NMS)_{exp}$	$(IS-NMS)_{calc}$	Exp.-Calc.
$5d^9 6s$	$^3D_2$ -	$5d^8 6s^2$	$^3F_4$	-86.0(6)	-86.0	0
$5d^9 6s$	$^3D_3$ -	$5d^8 6s^2$	$^3F_3$	-121.2(7)	-121.2	0
$5d^8 6s^2$	$^3F_3$ -	$5d^8 6s^2$	$^3F_4$	4.9(1.0)	5.0	-0.1
$5d^9 6s$	$^3D_2$ -	$5d^9 6s$	$^1D_2$	-9.3(2.5)	-8.9	-0.4
$5d^9 6s$	$^3D_3$ -	$5d^9 6s$	$^1D_2$	-39.0(1.2)	-39.1	0.1

Table 9:

Results of the King plots transition i plotted against j. Columns 1 and 3 give the values of the slope, columns 2 and 4 those of the intersection points.

Transition i,j	F_i/F_j [a]	ΔSMS [a] [10^{-3} cm^{-1}]	F_i/F_j [b]	ΔSMS [b] [10^{-3} cm^{-1}]
306.5,299.8	1.28(10)	0.1(4.4)	1.268(29)	-0.07(1.39)
306.5,304.3	1.90(5)	-2.1(2.5)	1.923(34)	-0.53(1.68)
299.8,304.3	1.57(6)	2.6(3.4)	1.519(24)	-0.46(1.43)
299.8,300.2	2.74(9)	13.8(5.2)	2.657(47)	8.6(2.7)
306.5,300.2	3.33(11)	6.4(4.8)	3.363(64)	8.5(3.2)
304.3,300.2	1.73(4)	8.2(3.4)	1.747(18)	9.4(1.7)

[a] Fit to experimental data without constraints.

[b] Fit with the constraints of the SMSs in ns → np and ns^2 → nsnp transitions as estimated by Heilig and Steudel [39].

Table 10:

Relative nuclear charge radius parameter $\lambda^{A,A'}_{rel}$ of the stable Pt isotopes. The values from Ref. [35] are also normalized to the isotope pair ^{196,198}Pt.

λ_{rel}		
Isotope pair	This work	Ref. [35]
190,192	0.810(5)	0.835(29)
192,194	0.898(3)	0.894(10)
194,196	0.926(4)	0.923(3)
196,198	1.000	1.000
194,195	0.424(2)	0.421(5)

FIGURE CAPTION

Figure 1 Part of the level scheme of Pt I. Thick lines indicate the transitions studied by laser spectroscopy in the present work. The other transitions were studied by interference spectroscopy (continuous lines: this work, dashed lines: earlier work). The numbers given in parentheses are the branching ratios determined by Lotrian et al. [8]. Lifetimes are included as far as they are available [8, 9]. The three lowest-lying fs levels are almost equally populated at the temperatures necessary to form an atomic beam.

Figure 2 Experimental setup for laser fluorescence spectroscopy of Pt in a thermal atomic beam at $\lambda \approx 300$ nm with frequency doubling in an external ring cavity.
DAC: digital-to-analog converter. VFC: voltage-to-frequency converter

Figure 3 Fluorescence spectrum of stable Pt isotopes in the transition at $\lambda = 306.47$ nm. The inset shows the signal of the least abundant isotope ^{190}Pt (together with ^{192}Pt) magnified by a factor of 500.

Figure 4 King plot of the IS values in the transitions with λ306.47 nm and λ299.79 nm related to the isotope pair ^{194,196}Pt. The straight-line fit has been carried out by using all even-isotope pairs.

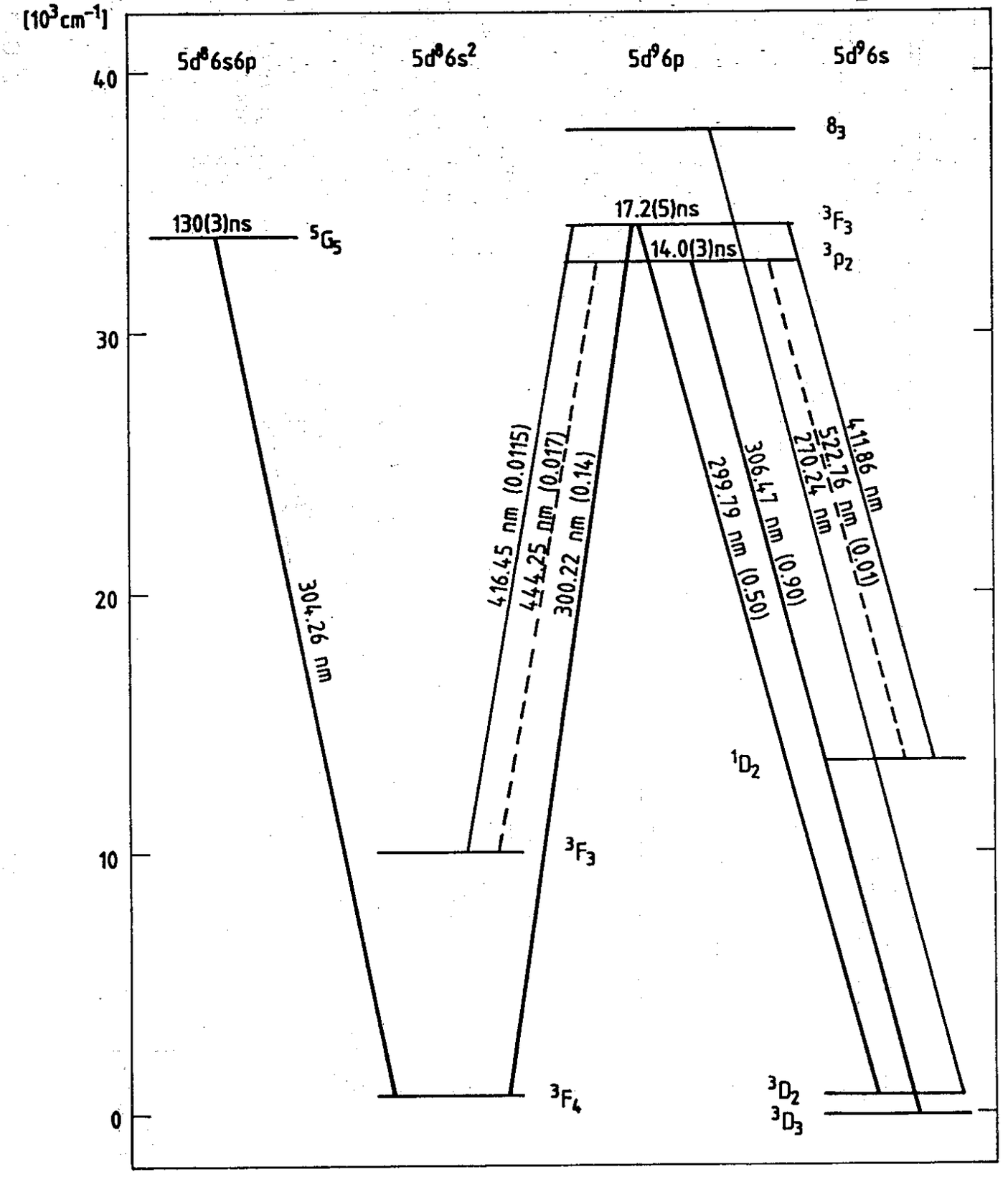
[10³cm⁻¹]
5d⁸6s6p
5d⁸6s²
5d⁹6p
5d⁹6s
40
30
20
10
0
130(3)ns
⁵G₅
304.26 nm
³F₄
416.45 nm (0.0115)
444.25 nm (0.017)
300.22 nm (0.14)
³F₃
8₃
17.2(5)ns
³F₃
14.0(3)ns
³P₂
299.79 nm (0.50)
306.47 nm (0.90)
522.76 nm
270.24 nm
411.86 nm (0.01)
¹D₂
³D₂
³D₃

FIG. 1

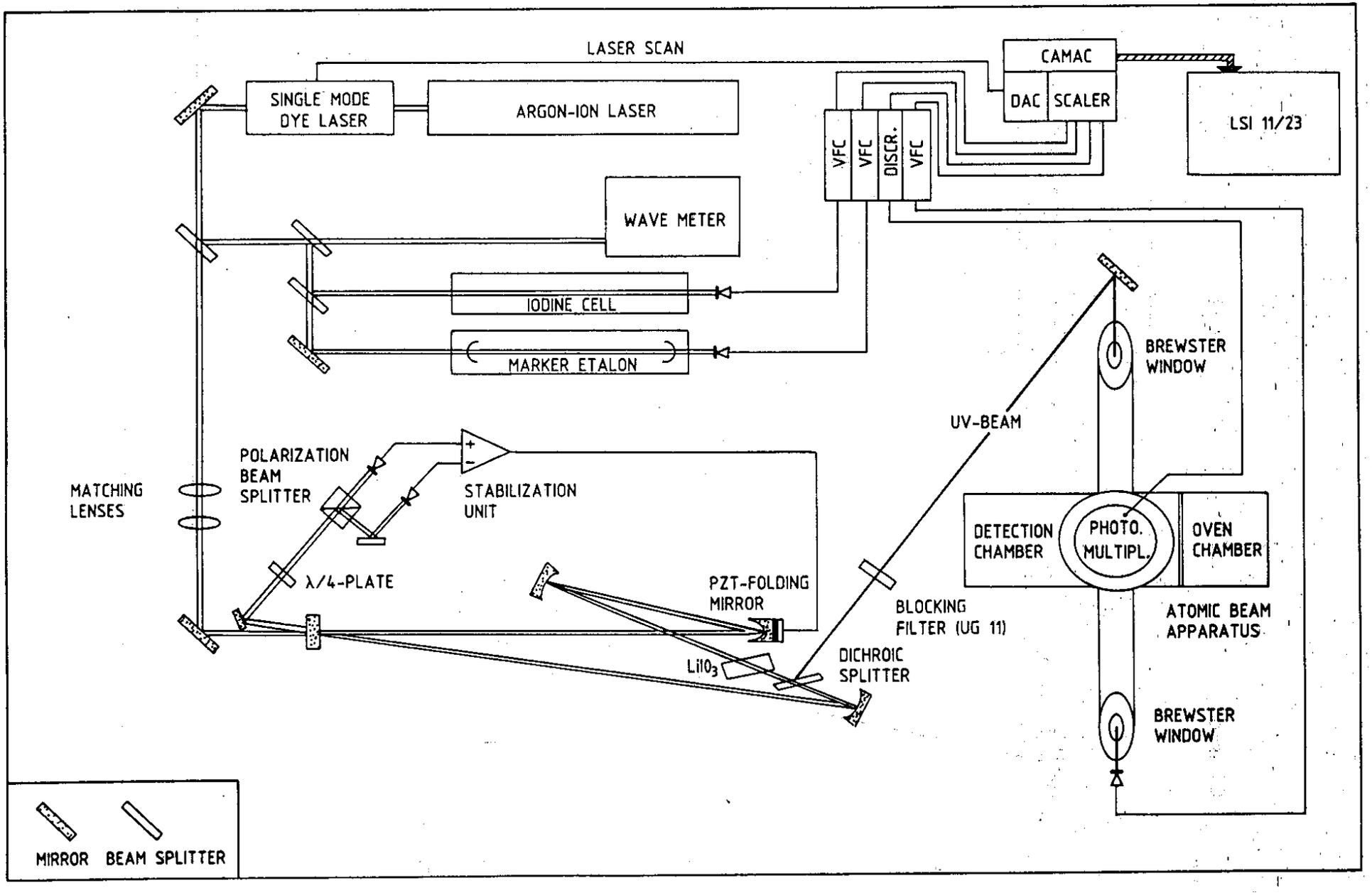
LASER SCAN
CAMAC
DAC
SCALER
LSI 11/23
SINGLE MODE DYE LASER
ARGON-ION LASER
VFC
VFC
DISCR.
VFC
WAVE METER
IODINE CELL
MARKER ETALON
BREWSTER WINDOW
UV-BEAM
MATCHING LENSES
POLARIZATION BEAM SPLITTER
STABILIZATION UNIT
DETECTION CHAMBER
PHOTO. MULTIPL.
OVEN CHAMBER
λ/4-PLATE
PZT-FOLDING MIRROR
BLOCKING FILTER (UG 11)
ATOMIC BEAM APPARATUS
LiIO3
DICHROIC SPLITTER
BREWSTER WINDOW
MIRROR
BEAM SPLITTER

FIG.2

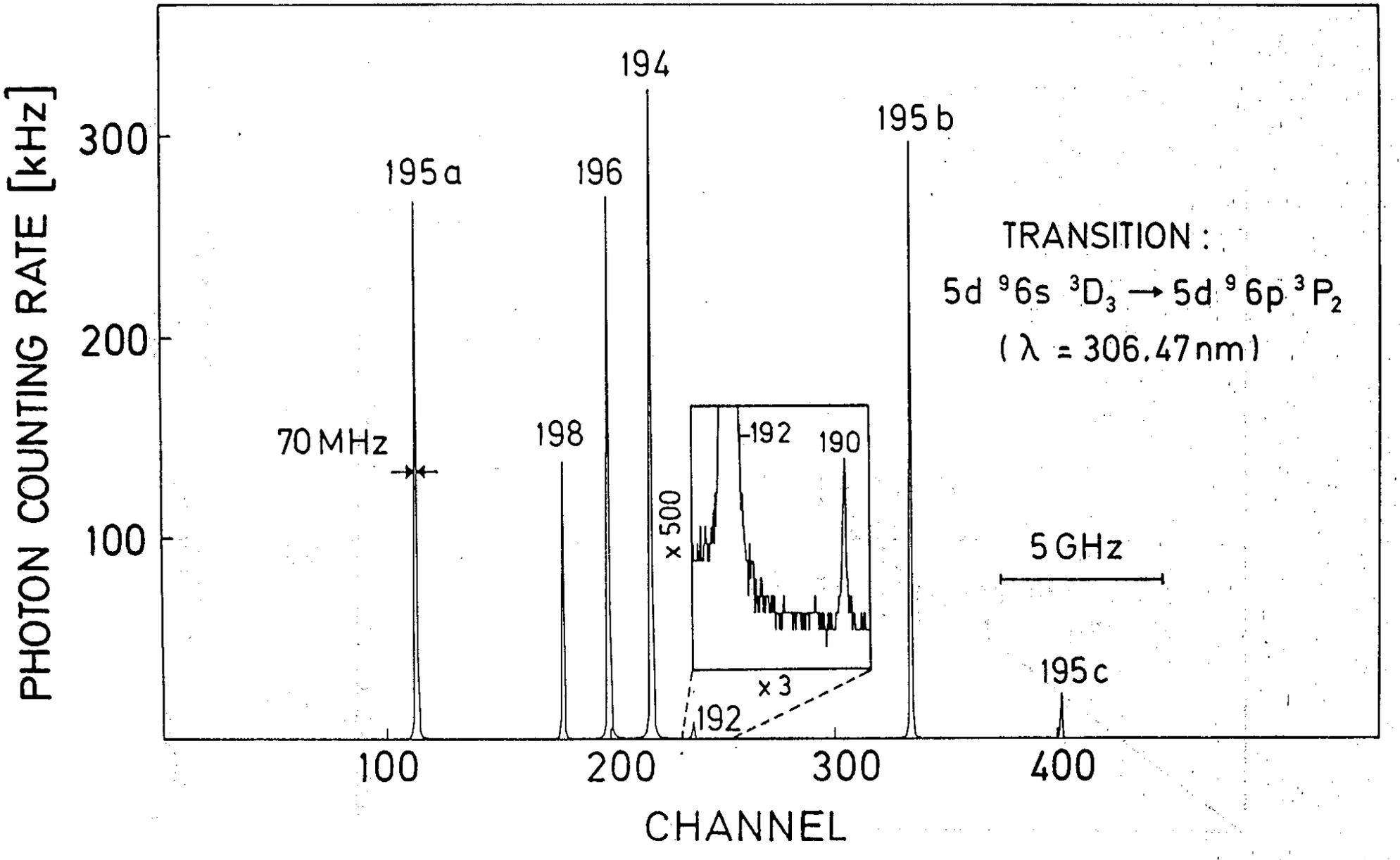
PHOTON COUNTING RATE [kHz]
300
200
100
195a
196
194
195b
198
70 MHz
192
190
x 500
x 3
192
TRANSITION :
5d ⁹6s ³D₃ → 5d ⁹6p ³P₂
(λ = 306.47nm)
5 GHz
195c
100
200
300
400
CHANNEL

FIG.3

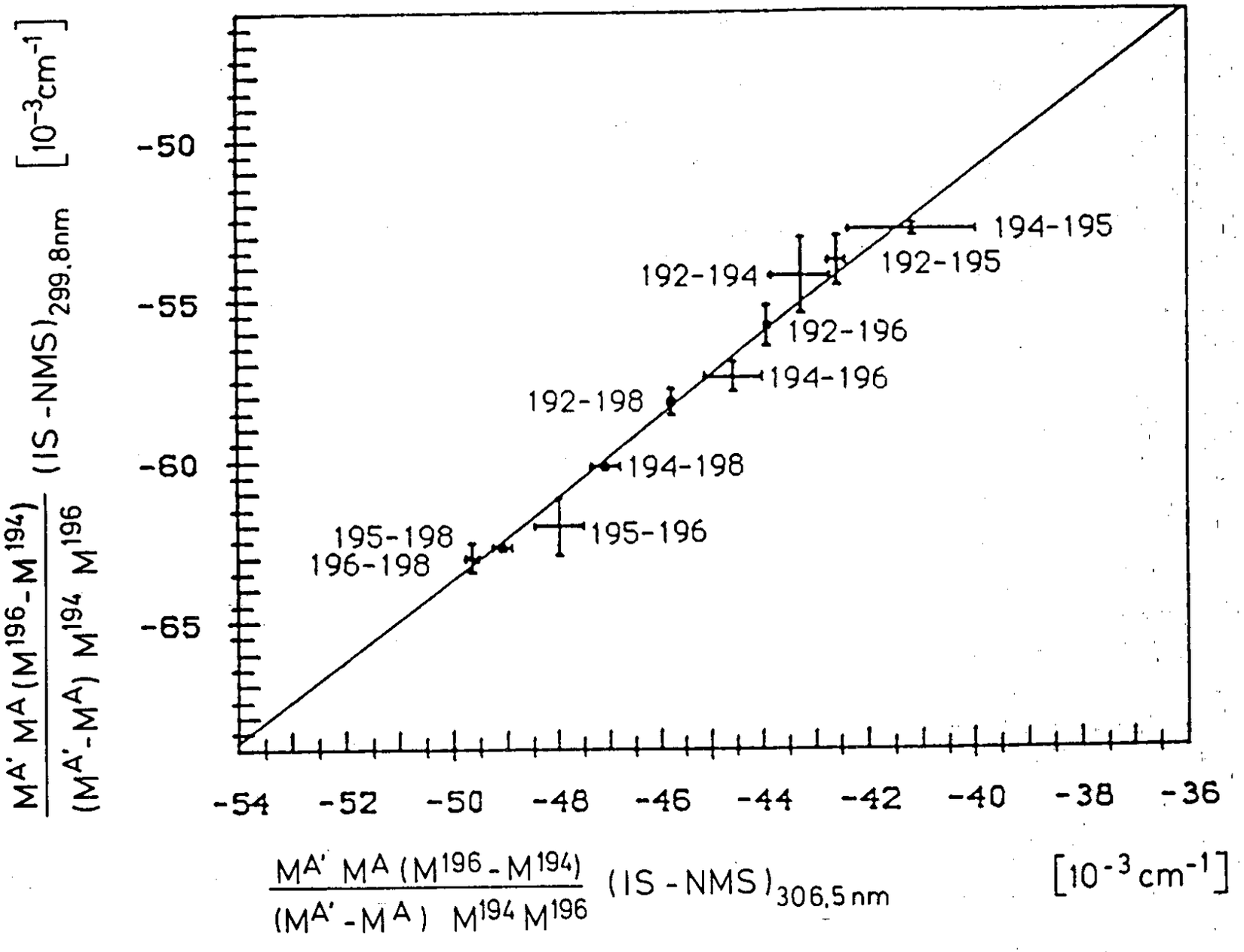
-50
-55
-60
-65
-54
-52
-50
-48
-46
-44
-42
-40
-38
-36
194-195
192-195
192-194
192-196
194-196
192-198
194-198
195-196
195-198
196-198
$\frac{M^{A'} M^{A} (M^{196} - M^{194})}{(M^{A'} - M^{A}) M^{194} M^{196}} (IS - NMS)_{299.8nm}$ $[10^{-3} cm^{-1}]$
$\frac{M^{A'} M^{A} (M^{196} - M^{194})}{(M^{A'} - M^{A}) M^{194} M^{196}} (IS - NMS)_{306.5nm}$ $[10^{-3} cm^{-1}]$

FIG. 4